Article

Theoretical Study of the Competition Mechanism of Alloying Elements in L1$_2$-(Ni$_{x1}$Cr$_{x2}$Co$_{x3}$)$_3$Al Precipitates

Yu Liu [1,2], Lijun Wang [1], Juangang Zhao [1], Zhipeng Wang [3], Touwen Fan [1], Ruizhi Zhang [1,*], Yuanzhi Wu [1,*], Xiangjun Zhou [1], Jie Zhou [1] and Pingying Tang [4]

[1] Research Institute of Automobile Parts Technology, Hunan Institute of Technology, Hengyang 421002, China; liuyu@hnit.edu.cn (Y.L.)
[2] College of Materials Science and Engineering, Hunan University, Changsha 410082, China
[3] State Key Laboratory of Advanced Design and Manufacturing for Vehicle Body, Hunan University, Changsha 410082, China
[4] Key Laboratory of New Electric Functional Materials of Guangxi Colleges and Universities, Nanning Normal University, Nanning 530023, China
[*] Correspondence: 2006000495@hnit.edu.cn (R.Z.); ranco007@163.com (Y.W.)

Abstract: The impact of variations in the content of single alloying element on the properties of alloy materials has been extensively discussed, but the influence of this change on the content of multiple alloying elements in the alloy materials has been disregarded, as the performances of alloy materials should be determined by the collective influence of multiple alloying elements. To address the aforementioned issue, the present study conducted a comprehensive investigation into the impact of variations in the content of alloying elements, namely Ni, Cr, and Co, on the structural and mechanical properties of L1$_2$-(Ni$_{x1}$Cr$_{x2}$Co$_{x3}$)$_3$Al precipitates using the high-throughput first-principles calculations and the partial least squares (PLS) regression, and the competitive mechanism among these three elements was elucidated. The findings demonstrate that the same alloying element may exhibit opposite effects in both single element analysis and comprehensive multi-element analysis, for example, the effect of Ni element on elastic constant C_{11}, and the influence of Cr element on Vickers hardness and yield strength. The reason for this is that the impact of the content of other two alloying elements is ignored in the single element analysis. Meanwhile, the Co element demonstrates a significant competitive advantage in the comparative analysis of three alloying elements for different physical properties. Therefore, the methodology proposed in this study will facilitate the elucidation of competition mechanisms among different alloy elements and offer a more robust guidance for experimental preparation.

Keywords: L1$_2$-precipitate; first-principles calculations; partial least squares regression; competitive mechanism

1. Introduction

Precipitation strengthening, which has been widely studied, is an important method for modulating alloy materials, which can achieve the goal of enhancing strength and toughness, thereby significantly improving the overall properties of alloys [1–5]. Affected by the type of element, crystal structure, and naming convention, the hardening particles exhibit a variety of γ' [6], γ'' [7], *Kanbanρ* [8], B2 [9], L1$_2$ [10], etc. The γ' precipitate strengthens alloy materials [11], increasing the yield strength and ultimate tensile strength of (FeCoNi)$_{81}$Cr$_9$Al$_8$Ti$_1$Nb$_1$ high-entropy alloy (HEA) to 863 MPa and 1285 MPa, respectively [12]. Due to the high thermodynamic stability and high-temperature strengthening effect of γ'' and B2 particles [13,14], the creep resistance of nickel-based superalloy Inconel 718 was significantly enhanced at 650 °C [15], and Ti-modified steels maintained their creep properties after being tested for 700 h at 700 °C [16]. The precipitation of *Kanbanρ* particles resulted in a remarkable peak hardness of 440 Hv at 800 °C for the CuCr$_2$Fe$_2$NiMn HEA [8],

while the precipitated phases significantly enhanced the tensile strength of other alloys without compromising their ductility [17]. Therefore, the precipitation strengthening is a crucial factor in enhancing the mechanical properties of alloys, and it is imperative and meaningful to investigate the precipitated phases.

Among these, the $L1_2$ nanoparticles exhibit an outstanding strengthening effect that has been extensively investigated by researchers. Sun et al. [18] developed a CoCrNi medium-entropy alloy with bimodal $L1_2$ precipitates to enhance the synergy between strength and ductility. The resulting alloy exhibited a yield strength of 1.16 GPa, a tensile strength of 1.55 GPa, and a uniform elongation of 28%, which was attributed to heterogeneous deformation-induced strengthening caused by the bimodal $L1_2$ nanoprecipitates. Wang et al. [19] utilized thermomechanical treatment to generate high-content $L1_2$ precipitates in $[(Al_{0.5}Ti_{0.5})-(FeCoNi)_{12}]Cr_3$ HEA, resulting in an improvement of the ultimate tensile strength and ductility of the alloy to 1356.5 MPa and 34.9%. Refining $L1_2$-Cr_3Cu particles was found to enhance the high-temperature strength of Cu-Cr-Nb alloy to 223 ± 5 MPa at 500 °C, as demonstrated by Yang et al. [20]. Furthermore, the $L1_2$ phase underwent a morphological transformation from individual particles to a tweed-like morphology, as observed by Strumza et al. [21], resulting in a significant increase in hardness from 218 Hv to 388.5 Hv when compared with the non-aged $Al_{0.5}CoCrFeNi$ HEA at 600 °C. Yamamoto et al. [22] promoted the formation of $L1_2$-ordered $Ni_3(Al,Ti)$ in $Fe_{14}Cr_{32}Ni_3Nb_{(3-4)}Al_{(1-3)}Ti$ (wt.%)-based alumina-forming austenitic stainless alloys, indicating a significant enhancement in the oxidation and creep resistance of alloys. Meanwhile, researchers found that Al-Zr-Y alloy had significantly higher conductivity than Al-Zr alloy due to larger volume $L1_2$-$Al_3(Zr,Y)$ precipitate formation [23]. Overall, the strengthening effects of $L1_2$ nanoparticles on alloy materials are diverse, and studying $L1_2$ particles is crucial for achieving breakthroughs in the physical properties of alloys.

However, there are still deficiencies in the current research on $L1_2$ precipitates. The aforementioned studies mainly focus on the influence of $L1_2$ particles on alloy mechanical properties, while lacking a detailed discussion of their own physical characteristics, particularly the competitive mechanism between alloying elements for mechanical properties. Therefore, in order to elucidate the competitive mechanism of alloying elements in $L1_2$ precipitates, this paper systematically investigates the effects of Ni, Cr, and Co contents on the mechanical properties of $L1_2$-$(Ni_{x1}Cr_{x2}Co_{x3})_3Al$ precipitates through high-throughput first-principles calculations using exact muffin-tin orbitals (EMTOs) and coherent potential approximation (CPA) methods, and the partial least squares (PLS) regression is subsequently employed to elucidate the extent of influence exerted by different elements on a specific physical property, thereby indicating the competitive mechanism among these elements. Herein, Ni, Cr, and Co are control variables in the alloy, with *x*1, *x*2, and *x*3 representing their respective contents from 0 to 75 at%, as the ratio of alloying elements on either side of $L1_2$-$(Ni_{x1}Cr_{x2}Co_{x3})_3Al$ precipitated phases is 3:1. Furthermore, the intrinsic properties such as lattice constant, elastic constants, elastic moduli, Vickers hardness, and yield strength are calculated, and the competitive mechanisms of alloying elements on these properties are discussed in detail.

2. Computational Details

In this work, the numerical relationships between alloying elements and the structural and mechanical properties of $L1_2$-$(Ni_{x1}Cr_{x2}Co_{x3})_3Al$ precipitates are obtained by the EMTO-CPA method based on the density functional theory (DFT) [24–26]. Herein, the Kohn–Sham equations [27,28] and full charge density technique [29] are chosen to solve the single-electron equations of optimized overlapping muffin-tin potential spheres and total energy, respectively. The generalized gradient approximation (GGA) within the Perdew–Burke–Ernzerhof (PBE) theory is utilized to symbolize the exchange–correlation functional [30], the disordered local moment model is exploited to characterize the paramagnetic state [31], and the $25 \times 25 \times 25$ inequivalent *k*-points for integration calculations are set to ensure the convergence accuracy of all energies in the Brillouin zone. Meanwhile, the convergence of

s, p, d, and f orbitals is optimized in the EMTO basis group [32], the electrostatic correction of single-site CPA method is executed by the screened impurity model with screening parameter 0.7 [33], and the atomic short-range order and local lattice relaxation effects are not considered [34]. Subsequently, to ensure the accuracy of calculated results, Green's function of 16 complex energy points on the Fermi surface is solved [35], the predicted energy–volume data are fitted by the Morse-type function [36] to acquire the equation of state, and then the equilibrium volume and lattice constant of L1$_2$-(Ni$_{x1}$Cr$_{x2}$Co$_{x3}$)$_3$Al precipitates are obtained.

Subsequently, the competitive mechanism among alloying elements is further elucidated by analyzing their impact on physical properties using the PLS regression [37]. The PLS regression is a cutting-edge multivariate statistical approach that integrates multiple linear regression analysis [38], canonical correlation analysis [39], and principal component analysis [40]. It effectively addresses the issues of multicollinearity, high-dimensional variables, and small sample sizes [41]. In this study, the alloying elements Ni, Cr, and Co are considered as control variables in the L1$_2$-(Ni$_{x1}$Cr$_{x2}$Co$_{x3}$)$_3$Al precipitates with a range of 0–75 at%, while maintaining a constant total content of 75 at% for these three elements. Moreover, one of the elements serves as the primary control variable and increases by 15 at%, while the other two act as slave variables with equivalent content values. For example, the black dash line with rectangular box in Figure 1, i.e., Ni, is the primary control variable, and its content C_{Ni} sequentially ranging from 0, 15, 30, 45, 60, and 75 at%. Cr and Co are the slave variables, with their contents are determined by C_{Ni} as $C_{Cr} = C_{Co} = (75 \text{ at\%} - C_{Ni})/2$. Table 1 displays the alterations in Ni, Cr, and Co content during the calculation process, indicating that the limitations stem from a small sample size, independent variable correlation, and prediction of multiple dependent variables. Therefore, this issue is applicable to the establishment of regression models by the PLS method through analysis of the impact of each alloying element on the intrinsic property of L1$_2$ precipitates. A larger standardized regression coefficient indicates a greater influence, revealing the competitive mechanism among alloying elements.
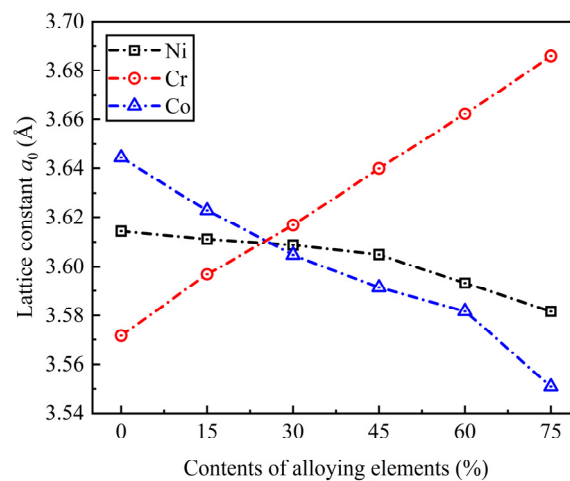

Figure 1. Dependencies of lattice constant a_0 on different Ni, Cr, and Co contents in L1$_2$-(Ni$_{x1}$Cr$_{x2}$Co$_{x3}$)$_3$Al precipitates.

Table 1. The variations in the content of Ni, Cr, and Co throughout the calculation process.

	Primary Control Variable Ni (at%)						Primary Control Variable Cr (at%)						Primary Control Variable Co (at%)					
C_{Ni}	0	15	30	45	60	75	37.5	30	22.5	15	7.5	0	37.5	30	22.5	15	7.5	0
C_{Cr}	37.5	30	22.5	15	7.5	0	0	15	30	45	60	75	37.5	30	22.5	15	7.5	0
C_{Co}	37.5	30	22.5	15	7.5	0	37.5	30	22.5	15	7.5	0	0	15	30	45	60	75

3. Results and Discussions

To investigate the competitive mechanisms of alloying elements on the intrinsic properties of L1$_2$-(Ni$_{x1}$Cr$_{x2}$Co$_{x3}$)$_3$Al precipitates, we first calculated the equilibrium lattice constant a_0 using the EMTO-CPA method, and the resulting variation curves of a_0 with respect to the alloying elements Ni, Cr, and Co for the L1$_2$ precipitates are depicted in Figure 1. It is noteworthy that the legend in the figure only lists the primary control variables Ni, Cr, and Co in each calculation process, while omitting the corresponding slave variables. Obviously, the a_0 value exhibits a negative correlation with increasing Ni or Co content, while it shows a positive correlation with increasing Cr content. The results indicate that increasing Ni or Co content in the L1$_2$-(Ni$_{x1}$Cr$_{x2}$Co$_{x3}$)$_3$Al precipitates will induce lattice reduction, while the opposite effect is observed with the Cr element, which is in line with the comparatively larger atomic radius of the Cr element and the relatively smaller atomic radii of Ni and Co elements. Meanwhile, it can be found that the impact of Ni and Co on the lattice constant a_0 is different under identical negative action trends; the incorporation of higher Co content results in a more rapid reduction in the a_0 value, showing that the lattice constant of L1$_2$-(Ni$_{x1}$Cr$_{x2}$Co$_{x3}$)$_3$Al particles exhibits a more pronounced decrease with an increase in Co content compared to an increase in Ni content. However, according to the principle of decreasing atomic radius from left to right within a period, the Co element exhibits a larger atomic radius than the Ni element, and there appears to be a discrepancy between the aforementioned conclusion and the principle.

To further investigate the underlying factors, we employed the PLS regression to gather additional information [37] because it is insufficient to solely analyze the impact of a single alloying element on the lattice constant a_0 based on Figure 1 alone. The alteration in the primary control variable leads to a corresponding modification in the slave control variables, as listed in Table 1. Therefore the effect on a_0 is a result of the synergistic interaction among the alloying elements Ni, Cr, and Co, and the influence of each element on a_0 exhibits distinct variations. Accordingly, for the calculation process of PLS regression, the optimal number of principal components is firstly determined as 1 through cross-validation analysis based on the data results in Figure 1 and Table 1, and the subsequent regressive analysis is conducted to elucidate the distinct impacts of alloying elements on lattice constant a_0. The corresponding computed outcomes are listed in Table 2.

Table 2. The PLS regression results for the content of alloying elements Ni, Cr, and Co, and the lattice constant a_0.

Independent Variables	Dependent Variable	Standardized Regression Coefficients	Projected Importance Indexes	R^2 Value (%)
C_{Ni}		−0.187	0.400	
C_{Cr}	a_0	0.643	1.375	98.4
C_{Co}		−0.456	0.974	

In Table 2, a_0 is considered the dependent variable, while the concentrations of Ni, Cr, and Co are regarded as the independent variables. By calculation, the standardized regression coefficients, respectively, are −0.187, 0.643, and −0.456, meaning that the standardized regression relationship between the dependent variable a_0 and the independent variables C_{Ni}, C_{Cr}, and C_{Co} can be expressed as $a_0 = -0.187C_{Ni} + 0.643C_{Cr} - 0.456C_{Co}$. The regression coefficient values independently reflect the extent of influence exerted by the corresponding alloying elements on a_0, and the larger the absolute value of the coefficient, the more significant its impact becomes. The positive and negative signs in this context signify the directional influence of these three alloying elements. Meanwhile, the bar chart presented in Figure 2 offers a visual representation of the varying magnitudes of impact, facilitating intuitive comprehension and enhancing the clarity and precision of our findings. Evidently, a_0 is influenced differently by the three alloying elements, with Cr exhibiting the most pronounced effect and Ni exerting the least impact. The observed trend aligns with the established order of atomic radius magnitudes for the alloy constituents

Ni, Cr, and Co. The result also reveals a positive correlation between the lattice constant of L1$_2$-(Ni$_{x1}$Cr$_{x2}$Co$_{x3}$)$_3$Al precipitates and the atomic radius of their alloying elements. Simultaneously, the projected importance indexes of 0.400, 1.375, and 0.974 in the table respectively indicate the explanatory ability of their corresponding independent variables towards the dependent variable. It can be seen that the explanatory ability of Cr and Co is relatively high, whereas that of Ni is comparatively low. Furthermore, the R^2 value reflects the level of goodness-of-fit of the PLS regression model; the fitted regression equation demonstrates a remarkable ability to account for 98.4% of the variability observed in the dependent variable.
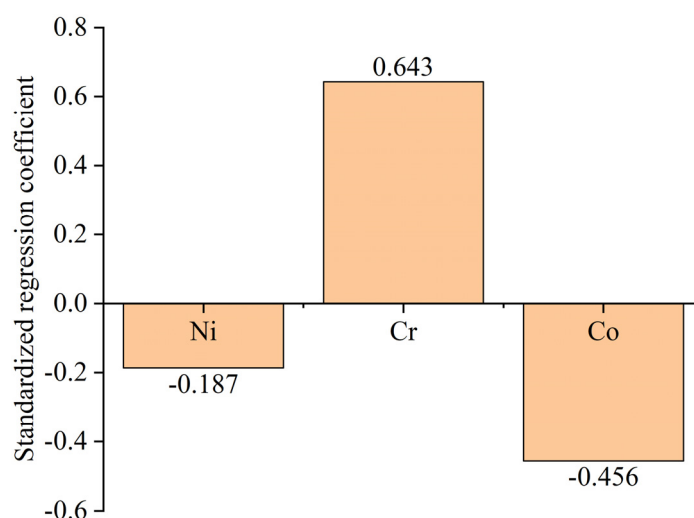

Figure 2. Histogram depicting the standardized regression coefficients of alloying elements Ni, Cr, and Co in relation to the lattice constant a_0.

The elastic constants C_{11}, C_{12}, and C_{44} of L1$_2$ particles are subsequently computed, as illustrated in Figure 3. Obviously, the curves in Figure 3a,c exhibit a certain degree of regularity as a whole, whereas the curves in Figure 3b lack any discernible pattern. C_{11} consistently exhibits an upward trend with the incorporation of alloying elements such as Ni, Cr, or Co, and the trend is positively correlated with the concentration of one of the elements, whereby higher concentrations yield increased values for C_{11} and lower concentrations result in decreased values, as shown in Figure 3a. The results demonstrated that the alloying elements Ni, Cr, and Co represent a similar enhancing effect on the elastic constant C_{11}, albeit with slight variations in their respective magnitudes of impact. The C_{44} value gradually increases with increasing Cr or Co content, while it initially rises and subsequently declines with the increase of Ni content, as displayed in Figure 3c. This indicates that the enhancement of C_{44} can be achieved by increasing the content of Cr or Co in the L1$_2$ particles, while the promoting effect of Co is more rapid compared to that of Cr, and a contrasting trend is observed with high contents of the Ni element. Meanwhile, the fluctuation in the C_{12} value does not follow a clear rule, with similar roles of Ni and Co elements observed. Specifically, the C_{12} value initially decreases and then increases with increasing Ni or Co content, while the role of the Co element is relatively chaotic. The aforementioned results primarily address the impact of individual element growth, while neglecting the assessment of the competitive trend posed by multi-alloying elements. Therefore, further investigation of this matter is warranted.
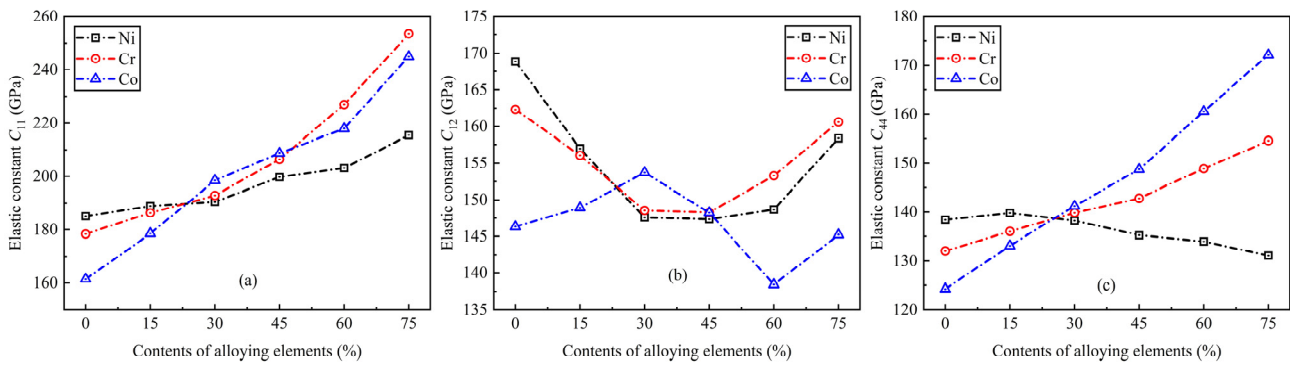
Figure 3. Dependencies of elastic constants C_{ij} on different Ni, Cr, and Co contents in L1$_2$-(Ni$_{x1}$Cr$_{x2}$Co$_{x3}$)$_3$Al precipitates: (**a**) designates C_{11}, (**b**) represents C_{12}, (**c**) implies C_{44}.

The influence of three alloying elements Ni, Cr, and Co on the elastic constants C_{11}, C_{12}, and C_{44} is further examined through PLS regression, with the calculated results tabulated in Table 3. It should be noted that the regression analysis of C_{11}, C_{12}, and C_{44} is performed individually in this study because there is no causal relationship among the three dependent variables; thus, the optimal number of principal components in the regression analysis for each data set was confirmed to be 1. The principles apply to all subsequent regression analyses with dependent variables and will not be further elaborated upon. Based on the computational findings, the standardized regression relationships between the dependent variables C_{11}, C_{12}, C_{44} and the independent variables C_{Ni}, C_{Cr}, C_{Co} are as follows:

$$\begin{cases} C_{11} = -0.442C_{Ni} + 0.330C_{Cr} + 0.281C_{Co} \\ C_{12} = -0.118C_{Ni} + 0.262C_{Cr} - 0.244C_{Co} \\ C_{44} = -0.467C_{Ni} + 0.234C_{Cr} + 0.233C_{Co} \end{cases} \quad (1)$$

in which the constant coefficients represent the standardized regression coefficients that were calculated, and the numerical values reflect the influence of the competitive relationship among the three alloying elements on the elastic constants, indicating that the magnitude and direction of the influence are different.

Table 3. The PLS regression results for the content of alloying elements Ni, Cr, and Co, and the elastic constants C_{ij}.

Independent Variables	Dependent Variables			Standardized Regression Coefficients			Projected Importance Indexes			R^2 Values (%)		
C_{Ni}				−0.442	−0.118	−0.467	1.013	0.247	1.268			
C_{Cr}	C_{11}	C_{12}	C_{44}	0.330	0.262	0.234	0.763	1.091	0.591	73.2	27.1	90.6
C_{Co}				0.281	−0.244	0.433	0.650	0.945	1.177			

To visually observe the distinct trend of this influence, the corresponding histogram of standardized regression coefficients is depicted in Figure 4. Obviously, the effect of Ni on C_{11} and C_{44} is observed to be more pronounced in a negative manner, and Cr exhibits a stronger positive impact on C_{12} compared to the other two elements. This observation suggests that one of the three alloy elements possesses a more pronounced competitive advantage in relation to the corresponding elastic constant. Furthermore, the coefficients corresponding to the Ni element consistently exhibit negative values, while those corresponding to the Cr element consistently demonstrate positive values. This indicates that the addition of the Ni element is not conducive to increasing the values of C_{11}, C_{12}, and C_{44}, whereas the inclusion of the Cr element facilitates an enhancement in these elastic constants. At the same time, the values of projected importance indexes in Table 3 respectively represent the explanatory ability of the independent variable towards

the corresponding dependent variable; the higher the value, the stronger the explanatory power, and the magnitude of the value corresponds to the absolute value of the regression coefficient. Moreover, the fitting quality of the regression equation should be further assessed by combining the R^2 value. In light of the calculated results, the R^2 values corresponding to C_{11}, C_{12}, and C_{44} are, respectively, 73.2%, 27.1%, and 90.6%. This indicates that the regression equations corresponding to C_{11} and C_{44} exhibit a good fit, whereas the regression equations associated with C_{12} demonstrate a poor fit. The perplexing relationship between the dependent variable C_{12} and the independent variables C_{Ni}, C_{Cr}, and C_{Co} gives rise to this phenomenon, as shown in Figure 3b. Therefore, the credibility of the regression equation for C_{12} in Equation (1) is questionable.
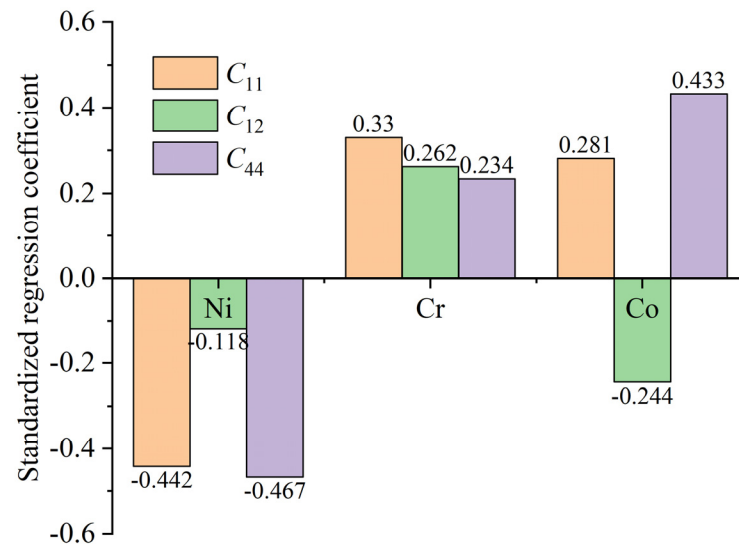

Figure 4. Histogram depicting the standardized regression coefficients of alloying elements Ni, Cr, and Co in relation to the elastic constants C_{ij}.

To investigate the competitive relationship among alloying elements Ni, Cr, and Co on the mechanical properties of L1$_2$-(Ni$_{x1}$Cr$_{x2}$Co$_{x3}$)$_3$Al precipitates, the elastic moduli, including bulk modulus B, shear modulus G, and Young's modulus E, of the L1$_2$ particles were further determined based on the obtained elastic constants [42], and the corresponding values are illustrated in Figure 5. It can be seen that the values of G and E exhibit a clear correlation with the increase in alloying element content, and demonstrate a similar trend. The values of two elastic moduli gradually increase with the rise in Cr or Co content, and the impact of the Co element on this growth trend becomes more pronounced, whereas the values of G and E exhibit an initial increase followed by a gradual decrease as the Ni content increases, but the decreasing trend is not statistically significant. Meanwhile, for the black curves in Figure 5b,c, when the content of the primary control element Ni is zero and the corresponding contents of the slave elements Cr and Co are both 37.5 at%, the alloy exhibits relatively large G and E values. For the blue curves in the figures, the G and E values of alloy are low when the content of the primary control element Co is 0 at%. A similar phenomenon is observed when the content of the primary control element is high. The commonality lies in the fact that the G and E values are higher with a low Ni content and a high Co content. The results demonstrate that the Co element exhibits a significantly favorable competitive advantage in terms of the overall generation of shear modulus G and Young's modulus E for L1$_2$ precipitates, whereas the Ni element demonstrates an unfavorable competitive advantage on the whole. The internal relationship of this competitive mechanism necessitates further investigation. Moreover, the curves in Figure 5a are messy and irregular. It can be found that the value of bulk modulus B decreases first and then increases with the increase in Ni or Cr content, while generally displaying an upward trend with increasing Co content. The L1$_2$ precipitates show a

higher *B* value when the content of the primary control element Ni is 0 at% or Cr is 75 at%. Furthermore, the *B* values corresponding to the three curves exhibit a relatively small discrepancy, which leads to confusion in interpretation when the contents of primary control elements are positioned in the middle. Therefore, the curves corresponding to *B* are relatively chaotic, which will not be conducive to exploring the competitive relationship between alloy elements Ni, Cr, and Co.
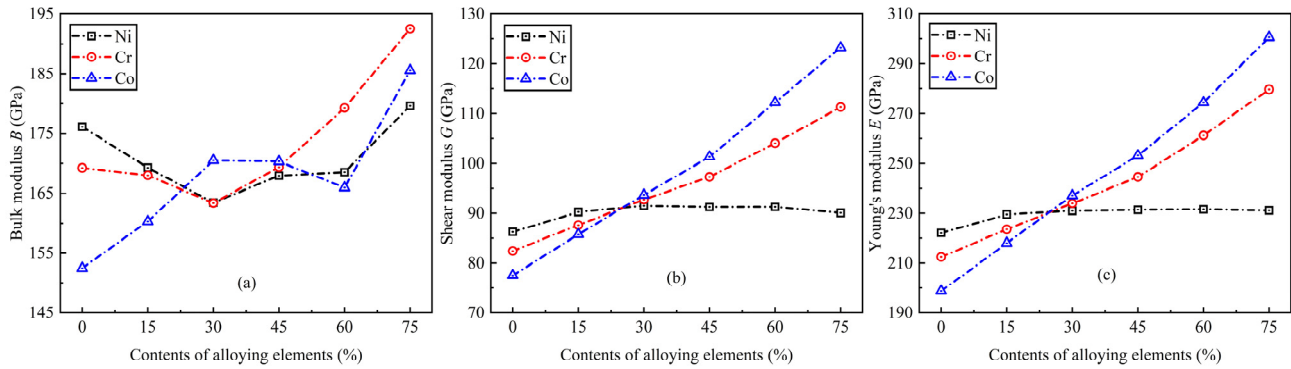

Figure 5. Dependencies of elastic moduli on different Ni, Cr, and Co contents in L1$_2$-(Ni$_{x1}$Cr$_{x2}$Co$_{x3}$)$_3$Al precipitates: (**a**) designates bulk modulus *B*, (**b**) represents shear modulus *G*, (**c**) implies Young's modulus *E*.

To explore the deeper competition mechanism, we conducted PLS regression analysis on the data derived from the aforementioned calculation, and the analysis results are listed in Table 4. According to the predicted values of standardized regression coefficients, a regression relationship between the elastic moduli *B*, *G*, and *E*, and the alloying element contents C_{Ni}, C_{Cr}, and C_{Co}, can be established as follows:

$$\begin{cases} B = -0.223C_{Ni} + 0.192C_{Cr} + 0.152C_{Co} \\ G = -0.479C_{Ni} + 0.157C_{Cr} + 0.426C_{Co} \\ E = -0.478C_{Ni} + 0.173C_{Cr} + 0.405C_{Co} \end{cases} \quad (2)$$

where the constant coefficients in front of the independent variables C_{Ni}, C_{Cr}, and C_{Co} are the corresponding standardized regression coefficients. The numerical values reflect the influence of the competitive relationship among the three alloying elements on the elastic moduli; the larger the coefficient's absolute value, the stronger the impact of the corresponding alloying element on the elastic modulus, reflecting that this alloying element possesses a superior competitive advantage compared to the other two alloying elements. Additionally, the positive and negative signs of the constant coefficients indicate the direction in which the alloying element promote or hinder the elastic modulus.

Table 4. The PLS regression results for the content of alloying elements Ni, Cr, and Co, and the elastic moduli.

Independent Variables	Dependent Variables			Standardized Regression Coefficients			Projected Importance Indexes			R^2 Values (%)		
C_{Ni}				−0.223	−0.479	−0.478	1.085	1.176	1.152			
C_{Cr}	*B*	*G*	*E*	0.192	0.157	0.173	0.740	0.283	0.306	24.7	88.0	86.2
C_{Co}				0.152	0.426	0.405	0.245	1.023	1.017			

Meanwhile, the histogram depicted in Figure 6 concisely presents the regression coefficients, providing a more in-depth description of the competitive relationship among different alloy elements. Obviously, the absolute value of regression coefficient corresponding to the Ni element is relatively large for each elastic modulus, indicating that Ni exhibits

a more pronounced competitive advantage compared to the other two elements in influencing the formation of elastic moduli B, G, and E of L1$_2$-(Ni$_{x1}$Cr$_{x2}$Co$_{x3}$)$_3$Al precipitates. However, the impact of the Ni element is negative, and the influence of Cr and Co elements is positive. These results suggest that enhancing the elastic moduli of L1$_2$ precipitates should be achieved by increasing the Cr and Co contents while reducing the Ni content. Moreover, the projected importance indexes in Table 4 denote the explanatory ability of the independent variable towards the corresponding dependent variable, and the ranking of index values aligns consistently with the ranking of the absolute value of their corresponding regression coefficient, which is positively correlated with the explanatory ability of alloying elements in the regression equation. However, the R^2 value between the dependent variable B and the independent variables C_{Ni}, C_{Cr}, and C_{Co} is 24.7%, which is relatively small because the curve relationship between the two parties is a significant irregularity in Figure 5a, indicating that the regression equation $B = -0.223C_{Ni} + 0.192C_{Cr} + 0.152C_{Co}$ is not reliable. Furthermore, the other two R^2 values are 88.0% and 86.2%, respectively, suggesting that the regression analysis results of G and E are noteworthy references in this study.
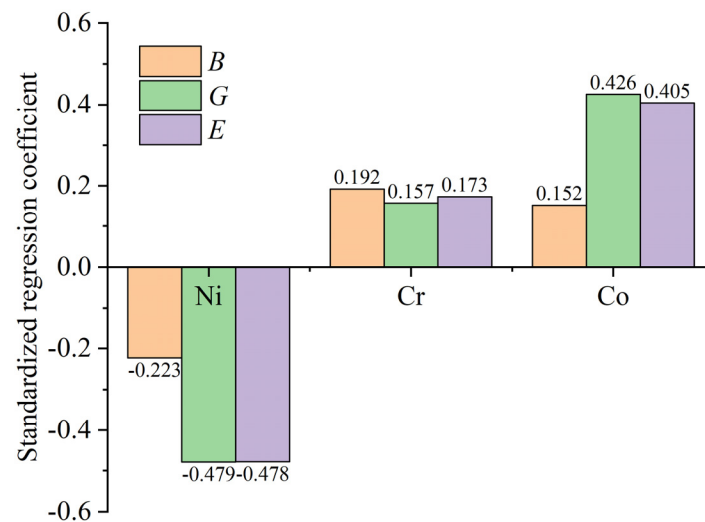

Figure 6. Histogram depicting the standardized regression coefficients of alloying elements Ni, Cr, and Co in relation to the elastic moduli.

Finally, Vickers hardness H_v and yield strength σ_y were calculated to further investigate the competitive mechanisms of alloying elements on mechanical properties of L1$_2$-(Ni$_{x1}$Cr$_{x2}$Co$_{x3}$)$_3$Al precipitates, as shown in Figure 7. It should be noted that the calculation formulas for H_v and σ_y are, respectively, $H_v = 2\left(G^3/B^2\right)^{0.585}$ and $\sigma_y = H_v/3$, according to references [43,44]. Therefore the forms of curves in Figure 7a,b are similar. Clearly the values of H_v and σ_y increase with the increase in Cr or Co content, indicating that the incorporation of alloying elements Cr and Co facilitates the enhancement of H_v and σ_y. However, the promoting effect of the Co element becomes more pronounced when the Co content exceeds 30 at% because the corresponding curves have a larger growth amplitude, as shown by the blue curves in Figure 7. Meanwhile, the promoting effect of the Ni element on H_v and σ_y exhibits an initial increase followed by a subsequent decrease, with an inflection point observed at a Ni content of 30 at%. Furthermore, the B value increases with the increase in primary control elements in the range of 0–30 at%. During this phase, the alloying elements Ni, Cr, and Co coexist at relatively high concentrations. The results demonstrate that the three alloying elements exhibit comparable effects on H_v and σ_y, without any single element displaying a prominent competitive advantage. However, the exceptional competitive advantage becomes evident when the content of primary control elements exceeds 30 at%. It can be found that the values of H_v and σ_y significantly rise by increasing the content of the Co element, whereas the influence of the Ni element displays

an inverse relationship. This reflects the positive promoting effect of the Co element and the negative reducing effect of the Ni element, with the competitive strength of the Cr element between that of the other two elements. Hence, it can be anticipated that the concentration of the Ni or Co element at 30 at% will represent a critical point in determining the hardness and yield strength of L1$_2$-(Ni$_{x1}$Cr$_{x2}$Co$_{x3}$)$_3$Al precipitates. Establishing the veracity of this assertion requires further experimental verification.
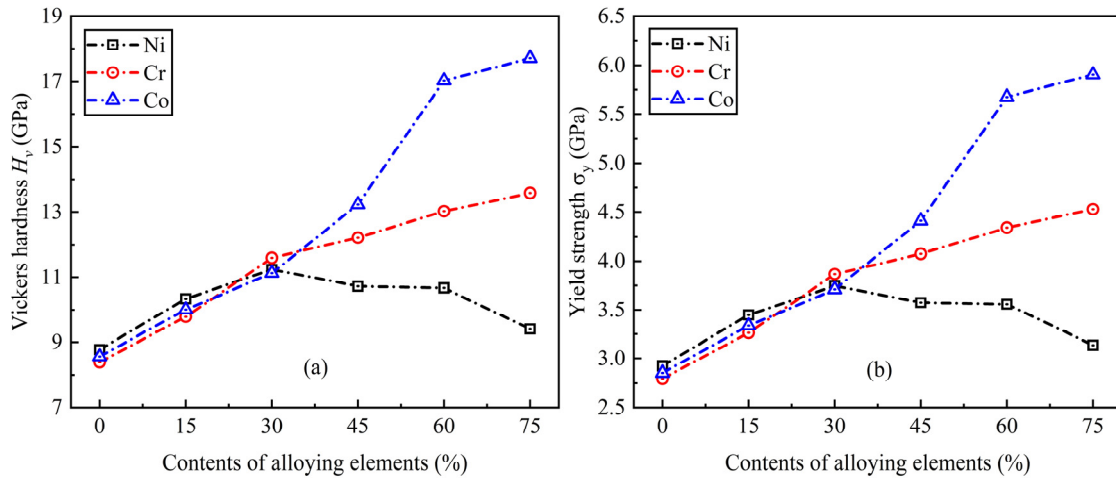
Figure 7. Dependencies of (**a**) Vickers hardness H_v and (**b**) yield strength σ_y on different Ni, Cr, and Co contents in L1$_2$-(Ni$_{x1}$Cr$_{x2}$Co$_{x3}$)$_3$Al precipitates.

In the light of the aforementioned calculation, the competitive relationship between alloying elements Ni, Cr, and Co in the mechanical properties of L1$_2$ precipitates was further analyzed using PLS regression; the analysis results are depicted in Table 5. It should be noted that the values of the regression analysis for H_v and σ_y are identical. The reason for this is that there is only a multiple relationship between H_v and σ_y, as mentioned previously. Drawing upon the computational findings, a standardized regression relationship between the dependent variables H_v and σ_y, and the independent variables C_{Ni}, C_{Cr}, and C_{Co}, can be established as follows:

$$\begin{cases} H_v = -0.472C_{Ni} - 0.107C_{Cr} + 0.479C_{Co} \\ \sigma_y = -0.472C_{Ni} - 0.107C_{Cr} + 0.479C_{Co} \end{cases} \quad (3)$$

in which the standardized regression coefficients are utilized as the constant coefficients. The coefficient value reflects the competitive relationship among the three alloying elements; the more pronounced the absolute value, the more formidable the competitive prowess, and the corresponding plus or minus sign denotes the direction of the influence on the Vickers hardness H_v and yield strength σ_y of L1$_2$ precipitates.

Table 5. The PLS regression results between the contents of Ni, Cr, and Co elements, and the Vickers hardness H_v and yield strength σ_y.

Independent Variables	Dependent Variables		Standardized Regression Coefficients		Projected Importance Indexes		R^2 Values (%)	
C_{Ni}			−0.472	−0.472	1.113	1.113		
C_{Cr}	H_v	σ_y	−0.107	−0.107	0.223	0.223	86.3	86.3
C_{Co}			0.479	0.479	1.136	1.136		

To clearly illustrate the competitive relationship, the regression coefficients for each alloying element are presented in Figure 8. Obviously, the Co element corresponds to the regression coefficients with the largest absolute values, suggesting that the Co element

has a greater competitive advantage on the Vickers hardness and yield strength of $L1_2$ particles compared with Ni and Cr elements. Additionally, the competitive advantage has a positive promoting effect on H_v and σ_y, because the coefficient values for the Co element are positive, whereas those for the Ni and Cr elements are negative. Furthermore, the Ni element exhibits a significantly negative regression coefficient of -0.472. The discrepancy between its absolute value and the regression coefficient corresponding to the Co element is negligible, suggesting that the Ni element also exhibits a significant negative competitive advantage in $L1_2$ particles. Therefore, it is imperative to consider the reverse interaction between Ni and Co elements when regulating the hardness and yield strength of $L1_2$-$(Ni_{x1}Cr_{x2}Co_{x3})_3Al$ precipitates.
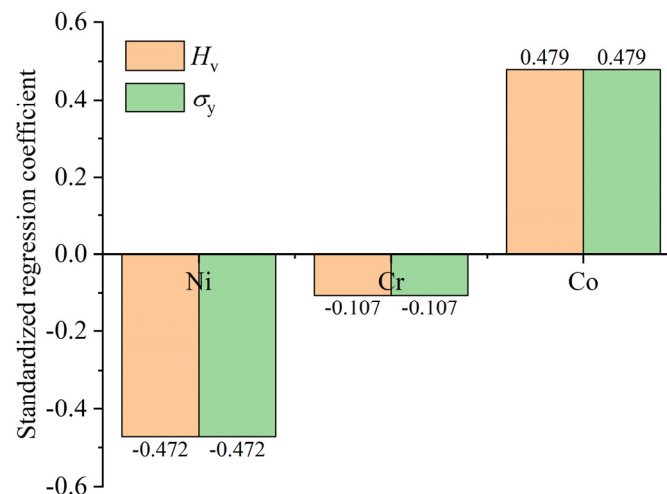
Figure 8. Histogram depicting the standardized regression coefficients of alloying elements Ni, Cr, and Co in relation to the Vickers hardness H_v and yield strength σ_y.

4. Conclusions

In this work, the EMTO-CPA method and PLS regression were employed to deeply investigate the impacts of the competitive mechanism of alloying elements Ni, Cr, and Co on the structural and mechanical properties of $L1_2$-$(Ni_{x1}Cr_{x2}Co_{x3})_3Al$ precipitates. The main conclusions are summarized as follows:

1. The competitive strength of Cr, Co, and Ni alloying elements decreased sequentially for the lattice constant a_0. Specifically, the Cr element exhibits a robust positive promoting effect while the Co and Ni elements exert an inverse influence.
2. The influence of the Ni element on the elastic constant C_{11} in the single curve analysis is opposite to that in the PLS regression analysis, with a positive correlation observed in the former and a negative correlation observed in the latter. The reason for this is that the single curve analysis solely focuses on variations in Ni content while disregarding the impact of Cr and Co content.
3. Through the overall analysis of PLS regression, Ni exhibits the most significant competitive advantage for the formation of B, G, and E in $L1_2$ particles. However, this competitive advantage manifests as negative effects, with respective values of -0.2223, -0.479, and -0.478. Conversely, Cr and Co elements demonstrate positive promoting effects on their respective competitive advantages.
4. When the content of Ni or Co element exceeds 30 at%, a significant variation in the Vickers hardness H_v and yield strength σ_y of $L1_2$ precipitates is observed. The potential critical points influencing the mechanical properties of $L1_2$ precipitates by the content of alloying elements were predicted. Furthermore, the Ni and Co elements exhibit a significant competitive advantage owing to their substantial standardized regression coefficients, although the effect is opposite.

References

1. Shan, L.Y.; Wang, X.L.; Chang, Y.L.; Wang, Y.P. Improving the mechanical performance of Cu-Cr alloy by dissolving Cu in the Cr second phase. *Mater. Charact.* **2021**, *176*, 111104. [CrossRef]
2. Cui, C.P.; Zhu, X.W.; Li, Q.; Zhang, M.; Zhu, G.P.; Liu, S.L. Study on high temperature strengthening mechanism of ZrO_2/Mo alloys. *J. Alloys Compd.* **2020**, *829*, 154630.
3. Hu, W.Q.; Du, Z.F.; Dong, Z.Z.; Yu, L.M.; Ahamad, T.; Ma, Z.Q. The synthesis of TiC dispersed strengthened Mo alloy by freeze-drying technology and subsequent low temperature sintering. *Scr. Mater.* **2021**, *198*, 113831. [CrossRef]
4. Lee, D.H.; Park, J.M.; Yang, G.H.; He, J.Y.; Lu, Z.P.; Suh, J.Y.; Kawasaki, M.; Ramamurty, U.; Jang, J. Nano-graining a particle-strengthened high-entropy alloy. *Scr. Mater.* **2019**, *163*, 24–28. [CrossRef]
5. Liu, Y.; Ye, T.; Zhou, Q.Y.; Wu, Y.Z.; Duan, S.Y.; Fan, T.W.; Wang, Z.P.; Tang, P.Y. High-throughput prediction of intrinsic properties of L1$_2$-(Ni$_{x1}$,Cr$_{x2}$,Co$_{x3}$)3(Al$_{y1}$,Ti$_{y2}$) precipitates. *Mater. Today Commun.* **2022**, *31*, 103655. [CrossRef]
6. Wang, C.L.; Liang, C.J.; Yang, M.J.; Huang, C.; Yao, Z.F.; Qiu, B.; Zhang, K.X.; Xie, Y.G.; Liang, M.L.; Liu, W.J.; et al. Development of the gamma′ phase strengthened high-temperature high-entropy alloys with excellent mechanical properties. *Mater. Des.* **2022**, *221*, 110940. [CrossRef]
7. Pan, Y.W.; Dong, A.P.; Zhou, Y.; Du, D.F.; Wang, D.H.; Zhu, G.L.; Sun, B.D. Enhanced strength-ductility synergy in a novel V-containing γ''-strengthened CoCrNi-based multi-component alloy. *Mater. Sci. Eng. A* **2021**, *816*, 141289. [CrossRef]
8. Ren, B.; Liu, Z.X.; Cai, B.; Wang, M.X.; Shi, L. Aging behavior of a CuCr$_2$Fe$_2$NiMn high-entropy alloy. *Mater. Des.* **2012**, *33*, 121–126. [CrossRef]
9. Qin, S.; Yang, M.X.; Jiang, P.; Wang, J.; Wu, X.L.; Zhou, H.; Yuan, F.P. Designing structures with combined gradients of grain size and precipitation in high entropy alloys for simultaneous improvement of strength and ductility. *Acta Mater.* **2022**, *230*, 117847. [CrossRef]
10. Du, X.H.; Li, W.P.; Chang, H.T.; Yang, T.; Duan, G.S.; Wu, B.L.; Huang, J.C.; Chen, F.R.; Liu, C.T.; Chuang, W.S.; et al. Dual heterogeneous structures lead to ultrahigh strength and uniform ductility in a Co-Cr-Ni medium-entropy alloy. *Nat. Commun.* **2020**, *11*, 2390. [CrossRef]
11. Balikci, E.; Raman, A. Characteristics of the γ' precipitates at high temperatures in Ni-base polycrystalline superalloy IN738LC. *J. Mater. Sci.* **2000**, *35*, 3593–3597. [CrossRef]
12. Li, Z.Y.; Fu, L.M.; Peng, J.; Zheng, H.; Ji, X.B.; Sun, Y.L.; Ma, S.; Shan, A. Improving mechanical properties of an FCC high-entropy alloy by γ' and B2 precipitates strengthening. *Mater. Charact.* **2020**, *159*, 109989. [CrossRef]
13. Sun, Z.Q.; Song, G.; Ilavsky, J.; Ghosh, G.; Liaw, P.K. Nano-sized precipitate stability and its controlling factors in a NiAl-strengthened ferritic alloy. *Sci. Rep.* **2015**, *5*, 16081. [CrossRef]
14. Zhou, H.C.; Lin, Y.J.; Chen, F.; Shen, Q. Effect of precipitation behavior on mechanical properties of a Nb-containing CoCrNi-based high-entropy alloy. *Met. Mater. Int.* **2022**, *29*, 674–692. [CrossRef]
15. Zhang, H.J.; Li, C.; Guo, Q.Y.; Ma, Z.Q.; Li, H.J.; Liu, Y.C. Improving creep resistance of nickel-based superalloy Inconel 718 by tailoring gamma double prime variants. *Scr. Mater.* **2019**, *164*, 66–70. [CrossRef]
16. Rawlings, M.J.S.; Liebscher, C.H.; Asta, M.; Dunand, D.C. Effect of titanium additions upon microstructure and properties of precipitation-strengthened Fe-Ni-Al-Cr ferritic alloys. *Acta Mater.* **2017**, *128*, 103–112. [CrossRef]

17. Xing, Z.Q.; Pang, J.Y.; Zhang, H.W.; Ji, Y.; Zhu, Z.W.; Wang, A.M.; Zhang, L.; Li, H.; Fu, H.M.; Zhang, H.F. Optimizing the microstructure and mechanical performance of Fe-Ni-Cr-Al high entropy alloys via Ti addition. *J. Alloys Compd.* **2023**, *943*, 169149. [CrossRef]

18. Sun, K.; Huang, P.; Wang, F. The bimodal nanocoherent precipitates leads to superior strength-ductility synergy in a novel CoCrNi-based medium entropy alloy. *J. Alloys Compd.* **2022**, *909*, 164809. [CrossRef]

19. Wang, F.P.; Wu, J.W.; Guo, Y.X.; Shang, X.J.; Zhang, J.; Liu, Q.B. A novel high-entropy alloy with desirable strength and ductility designed by multi-component substitution for traditional austenitic alloys. *J. Alloys Compd.* **2023**, *937*, 168266. [CrossRef]

20. Yang, Y.H.; Lei, Q.; Zhang, P.; Wang, W.Y.; Zhang, X.K.; Li, Y.P.; Zhou, K.C.; Li, Z. Stabilization of $L1_2$ structured Cr_3Cu precipitates in a Cu-4.06Cr-1.25Nb alloy with high high-temperature strength. *Mater. Res. Lett.* **2022**, *10*, 257–263. [CrossRef]

21. Strumza, E.; Ezersky, V.; Brosh, E.; Aizenshtein, M.; Hayun, S. The phase evolution and stability of $Al_{0.5}CoCrFeNi$ high-entropy alloy at 600 degrees C. *J. Alloys Compd.* **2022**, *927*, 167053. [CrossRef]

22. Yamamoto, Y.; Muralidharan, G.; Brady, M.P. Development of $L1_2$-ordered $Ni_3(Al,Ti)$-strengthened alumina-forming austenitic stainless steel alloys. *Scr. Mater.* **2013**, *69*, 816–819. [CrossRef]

23. Zhang, Y.Z.; Gao, H.Y.; Wang, Y.F.; Wang, J.; Sun, B.D.; Gu, S.W.; You, W.R. Effects of Y addition on microstructure and properties of Al-Zr alloys. *Trans. Nonferrous Met. Soc. China* **2014**, *24*, 2239–2243. [CrossRef]

24. Vitos, L. *Computational Quantum Mechanics for Materials Engineers: The EMTO Method and Applications*; Springer: London, UK, 2007.

25. Soven, P. Coherent-potential model of substitutional disordered alloys. *Phys. Rev.* **1967**, *156*, 809–813. [CrossRef]

26. Gyorffy, B.L. Coherent-potential approximation for a nonoverlapping-muffin-tin-potential model of random substitutional alloys. *Phys. Rev. B* **1972**, *5*, 2382–2384. [CrossRef]

27. Kohn, W.; Sham, L.J. Self-consistent equations including exchange and correlation effects. *Phys. Rev.* **1965**, *140*, 1133–1138. [CrossRef]

28. Vitos, L.; Kollar, J.; Skriver, H.L. Full charge-density calculation of the surface energy of metals. *Phys. Rev. B* **1994**, *49*, 16694–16701. [CrossRef] [PubMed]

29. Tian, F.; Varga, L.K.; Chen, N.; Delczeg, L.; Vitos, L. Ab initio investigation of high-entropy alloys of 3d elements. *Phys. Rev. B* **2013**, *87*, 075144. [CrossRef]

30. Perdew, J.P.; Burke, K.; Ernzerhof, M. Generalized gradient approximation made simple. *Phys. Rev. Lett.* **1996**, *77*, 3865–3868. [CrossRef]

31. Gyorffy, B.L.; Pindor, A.J.; Staunton, J.; Stocks, G.M.; Winter, H. A first-principles theory of ferromagnetic phase transitions in metals. *J. Phys. F Met. Phys.* **1985**, *15*, 1337–1386. [CrossRef]

32. Zoubi, N.I.A.; Punkkinen, M.P.J.; Johansson, B.; Vitos, L. Completeness of the exact muffin-tin orbitals: Application to hydrogenated alloys. *Phys. Rev. B* **2010**, *81*, 045122. [CrossRef]

33. Korzhavyi, P.A.; Ruban, A.V.; Abrikosov, I.A.; Skriver, H.L. Madelung energy for random metallic alloys in the coherent potential approximation. *Phys. Rev. B* **1995**, *51*, 5773–5780. [CrossRef] [PubMed]

34. Tian, F.; Varga, L.K.; Shen, J.; Vitos, L. Calculating elastic constants in high-entropy alloys using the coherent potential approximation: Current issues and errors. *Comput. Mater. Sci.* **2016**, *111*, 350–358. [CrossRef]

35. Tian, F.; Delczeg, L.; Chen, N.; Varga, L.K.; Shen, J.; Vitos, L. Structural stability of $NiCoFeCrAl_x$ high-entropy alloy from ab initio theory. *Phys. Rev. B* **2013**, *88*, 085128. [CrossRef]

36. Girifalco, L.A.; Weizer, V.G. Application of the morse potential function to cubic metals. *Phys. Rev.* **1959**, *114*, 687–690. [CrossRef]

37. Wold, S.; Sjostrom, M.; Eriksson, L. PLS-regression: A basic tool of chemometrics. *Chemom. Intell. Lab. Syst.* **2001**, *58*, 109–130. [CrossRef]

38. Faul, F.; Erdfelder, E.; Buchner, A.; Lang, A.G. Statistical power analyses using G*Power 3.1: Tests for correlation and regression analyses. *Behav. Res. Methods* **2009**, *41*, 1149–1160. [CrossRef]

39. Hardoon, D.R.; Szedmak, S.; Shawe-Taylor, J. Canonical correlation analysis: An overview with application to learning methods. *Neural Comput.* **2004**, *16*, 2639–2664. [CrossRef]

40. Wan, X.D.; Wang, Y.X.; Zhao, D.W. Multi-response optimization in small scale resistance spot welding of titanium alloy by principal component analysis and genetic algorithm. *Int. J. Adv. Manuf. Technol.* **2016**, *83*, 545–559. [CrossRef]

41. Chong, I.G.; Jun, C.H. Performance of some variable selection methods when multicollinearity is present. *Chemom. Intell. Lab. Syst.* **2005**, *78*, 103–112. [CrossRef]

42. Iotova, D.; Kioussis, N.; Lim, S.P. Electronic structure and elastic properties of the Ni_3X (X=Mn, Al, Ga, Si, Ge) intermetallics. *Phys. Rev. B Condens. Matter* **1996**, *54*, 14413–14422. [CrossRef] [PubMed]

43. Chen, X.Q.; Niu, H.Y.; Li, D.Z.; Li, Y.Y. Modeling hardness of polycrystalline materials and bulk metallic glasses. *Intermetallics* **2011**, *19*, 1275–1281. [CrossRef]

44. Pan, Y. Structural Prediction and Overall Performances of $CrSi_2$ Disilicides: DFT Investigations. *ACS Sustain. Chem. Eng.* **2020**, *8*, 11024–11030. [CrossRef]